A Fast Algorithm for High-Resolution Color Image Reconstruction with Multisensors

Michael K. Ng[*]   Wilson C. Kwan[†]   Raymond H. Chan[‡]

Abstract

This paper studies the application of preconditioned conjugate gradient methods in high resolution color image reconstruction problems. The high resolution color images are reconstructed from multiple undersampled, shifted, degraded color frames with subpixel displacements. The resulting degradation matrices are spatially variant. To capture the changes of reflectivity across color channels, the weighted H_1 regularization functional is used in the Tikhonov regularization. The Neumann boundary condition is also employed to reduce the boundary artifacts. The preconditioners are derived by taking the cosine transform approximation of the degradation matrices. We will show that the spectra of the preconditioned normal systems are clustered around 1 when the errors in the subpixel displacements are sufficiently small. Numerical examples are given to illustrate the fast convergence of the preconditioned conjugate gradient method.

1   Introduction

Using digital signal processing techniques to improve the spatial resolution of images, such as those obtained from satellites, is of great practical importance, see for instance [3, 12, 16, 18, 20, 21]. In this paper, we consider the reconstruction of high resolution color images from multiple undersampled, shifted, degraded and noisy color images which are obtained by using multiple identical color image sensors shifted from each other by subpixel displacements.

We remark that color can be regarded as a set of three images in their primary color components: red, green and blue. The reconstruction of high resolution color images can be modeled as solving

$$g = \mathcal{A}f + \eta, \tag{1}$$

where $\mathcal{A}$ is the reconstruction operator, η represents unknown Gaussian noise or measurement errors, g is the observed high resolution color image formed from the low resolution color images

---

and f is the desired high resolution color image. The observed and original color images can be expressed as

$$g = \begin{pmatrix} g^{(r)} \\ g^{(g)} \\ g^{(b)} \end{pmatrix}, \qquad f = \begin{pmatrix} f^{(r)} \\ f^{(g)} \\ f^{(b)} \end{pmatrix},$$

where $g^{(i)}$ and $f^{(i)}$ ($i \in \{r, g, b\}$) are the observed and the original color images from the red, green and blue channels respectively. The multichannel degradation operator $\mathcal{A}$ is given by

$$\mathcal{A} = \begin{pmatrix} \mathcal{A}^{rr} & \mathcal{A}^{rg} & \mathcal{A}^{rb} \\ \mathcal{A}^{gr} & \mathcal{A}^{gg} & \mathcal{A}^{gb} \\ \mathcal{A}^{br} & \mathcal{A}^{bg} & \mathcal{A}^{bb} \end{pmatrix}. \tag{2}$$

Here the operators $\mathcal{A}^{ii}$ and $\mathcal{A}^{ij}$ ($i \neq j$) represent the within-channel and the cross-channel degradation operators respectively.

Since the system (1) is ill-conditioned and generally not positive definite, we solve it by using a minimization and regularization technique:

$$\min_f \left\{ \sum_{i \in \{r,g,b\}} \alpha_i \left\| \sum_{j \in \{r,g,b\}} \mathcal{A}^{ij} f^{(j)} - g^{(i)} \right\|_2^2 + \mathcal{R}(f^{(r)}, f^{(g)}, f^{(b)}) \right\}. \tag{3}$$

Here $\mathcal{R}$ is a functional which measures the regularity of f and the regularization parameter α_i is to control the degree of regularity of the solution for the i-th channel. In this paper, we will use the weighted H_1 norm regularization functional [8] which can handle strong cross-channel correlations among color planes.

In the case of gray-level image reconstruction, we have already developed a fast algorithm that is based on the preconditioned conjugate gradient method with cosine transform preconditioners, see [5, 17]. In particular, we have shown that when the L_2 or H_1 norm regularization functional is used, the spectra of the preconditioned normal systems are clustered around one and hence the conjugate gradient method converges very quickly. For gray-level images, the use of the Neumann boundary condition can reduce the boundary artifacts and we have shown that solving such systems is much faster than solving those with zero and periodic boundary conditions, see the numerical results in [5, 17]. In the literature, the Neumann boundary condition has also been studied in image restoration [15, 1, 13] and in image compression [19, 14].

The main aim of this paper is to extend our results in [17] from grey-level images to color images which are vector-valued gray-level images. We will extend our fast and stable gray-level image processing algorithm with cosine transform preconditioners to the color image reconstruction problems. In particular, we will prove that when the weighted H_1 norm regularization functional is used, the spectra of the preconditioned systems are clustered around 1.

The outline of the paper is as follows. In Section 2, we give a mathematical formulation of the problem. In Section 3, we consider the image reconstruction problem when there are no error in the subpixel displacements. An introduction on the cosine transform preconditioners and the convergence analysis of our method will be given in Section 4. In Section 5, numerical results are presented to demonstrate the effectiveness of our method.

2 The Mathematical Model

We begin with a brief introduction of the mathematical model in high resolution image reconstruction. Details can be found in [3, 8, 11].

Consider a sensor array with $L_1 \times L_2$ sensors, each sensor has $N_1 \times N_2$ sensing elements (pixels) and the size of each sensing element is $T_1 \times T_1$. Our aim is to reconstruct an image of resolution $M_1 \times M_2$, where $M_1 = L_1 \times N_1$ and $M_2 = L_2 \times N_2$. To maintain the aspect ratio of the reconstructed image, we consider the case where $L_1 = L_2 = L$ only. For simplicity, we assume that L is an even number in the following discussion.

In order to have enough information to resolve the high resolution image, there are subpixel displacements between the sensors. In the ideal case, the sensors are shifted from each other by a value proportional to $T_1/L \times T_2/L$. However, in practice there can be small perturbations around these ideal subpixel locations due to imperfection of the mechanical imaging system. Thus, for $l_1, l_2 = 0, 1, \cdots, L-1$ with $(l_1, l_2) \neq (0, 0)$, the horizontal and vertical displacements $d^x_{l_1 l_2}$ and $d^y_{l_1 l_2}$ of the $[l_1, l_2]$-th sensor array with respect to the $[0, 0]$-th reference sensor array are given by

$$d^x_{l_1 l_2} = \frac{T_1}{L}(l_1 + \epsilon^x_{l_1 l_2}) \quad \text{and} \quad d^y_{l_1 l_2} = \frac{T_2}{L}(l_2 + \epsilon^y_{l_1 l_2}).$$

Here $\epsilon^x_{l_1 l_2}$ and $\epsilon^y_{l_1 l_2}$ denote respectively the normalized horizontal and vertical displacement errors.

We remark that the parameters $\epsilon^x_{l_1 l_2}$ and $\epsilon^y_{l_1 l_2}$ can be obtained by manufacturers during camera calibration. We assume that

$$|\epsilon^x_{l_1 l_2}| < \frac{1}{2} \quad \text{and} \quad |\epsilon^y_{l_1 l_2}| < \frac{1}{2}, \qquad 0 \leq l_1, l_2 \leq L - 1. \tag{4}$$

For if not, the low resolution images observed from two different sensor arrays will be overlapped so much that the reconstruction of the high resolution image is rendered impossible.

Let $f^{(r)}$, $f^{(g)}$ and $f^{(b)}$ be the original scene in red, green and blue channels respectively (cf. Figure 1 in §5 where the original scene from the three channels are combined). Then the observed low resolution image in the i-th ($i \in \{r, g, b\}$) channel $g^{(i)}_{l_1 l_2}$ for the (l_1, l_2)-th sensor is modeled by:

$$g^{(i)}_{l_1 l_2}[n_1, n_2] = \sum_{j \in \{r,g,b\}} w_{ij} \left\{ \int_{T_2(n_2 - \frac{1}{2}) + d^y_{l_1 l_2}}^{T_2(n_2 + \frac{1}{2}) + d^y_{l_1 l_2}} \int_{T_1(n_1 - \frac{1}{2}) + d^x_{l_1 l_2}}^{T_1(n_1 + \frac{1}{2}) + d^x_{l_1 l_2}} f^{(j)}(x_1, x_2) dx_1 dx_2 \right\} + \eta^{(i)}_{l_1 l_2}[n_1, n_2], \tag{5}$$

for $n_1 = 1, \ldots, N_1$ and $n_2 = 1, \ldots, N_2$ (cf. Figure 2 (left) and Figure 5 (left) in §5 where again the images from the three channels are combined). Here $\eta^{(i)}_{l_1 l_2}$ is the noise corresponding to the (l_1, l_2)-th sensor in the i-th channel, and w_{ii} and w_{ij} ($i \neq j$) are the within-channel and the cross-channel degradation parameters. We note that

$$w_{ij} \geq 0, \quad i, j \in \{r, g, b\} \quad \text{and} \quad \sum_{j=r,g,b} w_{ij} = 1, \quad i \in \{r, g, b\}. \tag{6}$$

3

To get the operator representation (1), we intersperse the low resolution images $g^{(i)}_{l_1 l_2}[n_1, n_2]$ to form an $M_1 \times M_2$ image by assigning

$$g^{(i)}[L(n_1 - 1) + l_1, L(n_2 - 1) + l_2] = g^{(i)}_{l_1 l_2}[n_1, n_2], \quad i \in \{r, g, b\}.$$

The image $g^{(i)}$ so formed is called the *observed high resolution image from the i-th channel* (cf. Figure 2 (right) and Figure 5 (right) in §5 which show the high resolution images after combining the images from all three channels). Similarly, we define $\eta^{(i)}$. Using a column by column ordering for $g^{(i)}$, $f^{(i)}$ and $\eta^{(i)}$, (5) becomes

$$g^{(i)} = \sum_{j \in \{r,g,b\}} w_{ij} \mathcal{H} f^{(j)} + \eta^{(i)}, \quad i \in \{r, g, b\}.$$

Writing it in operator form, we get (1) with $\mathcal{A}^{(ij)}$ in (2) given by

$$\mathcal{A}^{(ij)} = w_{ij} \mathcal{H}, \quad i, j \in \{r, g, b\}. \tag{7}$$

2.1 The Discrete Model

The continuous image model in (5) can be discretized by the rectangular rule and approximated by a discrete image model. Because (5) is a blurring process, the boundary values of $g^{(i)}$ are also affected by the values of $f^{(r)}$, $f^{(g)}$ and $f^{(b)}$ outside the scene. Thus in order to find f, we need some assumptions on the values of $f^{(r)}$, $f^{(g)}$ and $f^{(b)}$ outside the scene. Usual assumptions are the periodic boundary condition and the zero boundary condition. In [5], we proposed to use the Neumann boundary condition. It assumes that the scene immediately outside is a reflection of the original scene at the boundary. For grey-level image reconstruction problems, it gives better reconstructed images than that by the zero or periodic boundary conditions, see [5].

For $i \in \{r, g, b\}$, let $\mathbf{g}^{(i)}$ and $\mathbf{f}^{(i)}$ be respectively the discretization of $g^{(i)}$ and $f^{(i)}$ using a column by column ordering. Let

$$\mathbf{g} = [\mathbf{g}^{(r)} \ \mathbf{g}^{(g)} \ \mathbf{g}^{(b)}]^t \quad \text{and} \quad \mathbf{f} = [\mathbf{f}^{(r)} \ \mathbf{f}^{(g)} \ \mathbf{f}^{(b)}]^t.$$

Under the Neumann boundary condition assumption, the degradation matrices in each channel are banded matrices with bandwidth $2L - 1$, but there are entries added to the upper left part and the lower right part of the matrices (see the second matrix in (8)). The resulting matrices, denoted by $\mathbf{H}^x_{l_1 l_2}(\epsilon)$ and $\mathbf{H}^y_{l_1 l_2}(\epsilon)$, have a Toeplitz-plus-Hankel structure:

$$\mathbf{H}^x_{l_1 l_2}(\epsilon) = \frac{1}{L} \begin{pmatrix} 1 & \cdots & 1 & h^{x+}_{l_1 l_2} & & 0 \\ \vdots & \ddots & \ddots & \ddots & \ddots & \\ 1 & \ddots & \ddots & \ddots & \ddots & h^{x+}_{l_1 l_2} \\ h^{x-}_{l_1 l_2} & \ddots & \ddots & \ddots & \ddots & 1 \\ & \ddots & \ddots & \ddots & \ddots & \vdots \\ 0 & & h^{x-}_{l_1 l_2} & 1 & \cdots & 1 \end{pmatrix} + \frac{1}{L} \begin{pmatrix} 1 & \cdots & 1 & h^{x-}_{l_1 l_2} & & 0 \\ \vdots & \ddots & \ddots & & & \\ 1 & \ddots & & & & h^{x+}_{l_1 l_2} \\ h^{x-}_{l_1 l_2} & & & & \ddots & 1 \\ & & & \ddots & \ddots & \vdots \\ 0 & & h^{x+}_{l_1 l_2} & 1 & \cdots & 1 \end{pmatrix},$$

$$\tag{8}$$

4

and $\mathbf{H}_{l_1 l_2}^y(\epsilon)$ is defined similarly. The degradation matrix corresponding to the (l_1, l_2)-th sensor under the Neumann boundary condition is given by

$$\mathbf{H}_{l_1 l_2}(\epsilon) = \mathbf{H}_{l_1 l_2}^x(\epsilon) \otimes \mathbf{H}_{l_1 l_2}^y(\epsilon).$$

The degradation matrix for the whole sensor array is made up of degradation matrices from each sensor:

$$\mathbf{H}_L(\epsilon) = \sum_{l_1=0}^{L-1} \sum_{l_2=0}^{L-1} \mathbf{D}_{l_1 l_2} \mathbf{H}_{l_1 l_2}(\epsilon), \quad i, j \in \{r, b, g\}. \tag{9}$$

Here $\mathbf{D}_{l_1 l_2}$ are diagonal matrices with diagonal elements equal to 1 if the corresponding component of the observed low resolution image comes from the (l_1, l_2)-th sensor and zero otherwise, see [3] for more details. From (7), we see that we have the same matrix $\mathbf{H}_L(\epsilon)$ within the channels and across the channel, therefore by (2), the overall degradation matrix is given by

$$\mathbf{A}_L(\epsilon) = \begin{pmatrix} w_{rr} & w_{rg} & w_{rb} \\ w_{gr} & w_{gg} & w_{gb} \\ w_{br} & w_{bg} & w_{bb} \end{pmatrix} \otimes \mathbf{H}_L(\epsilon) \equiv \mathbf{W} \otimes \mathbf{H}_L(\epsilon). \tag{10}$$

In the next subsection, we will show that $\mathbf{A}_L(\epsilon)$ is ill-conditioned.

2.2 Ill-Conditioning of the Degradation Matrices

When there are no subpixel displacement errors, i.e., when all $\epsilon_{l_1, l_2}^x = \epsilon_{l_1, l_2}^y = 0$, the matrices $\mathbf{H}_{l_1 l_2}^x(0)$ and also $\mathbf{H}_{l_1 l_2}^y(0)$ are the same for all l_1 and l_2. We will denote them simply by $\mathbf{H}_L^x$ and $\mathbf{H}_L^y$. For instance, when $L = 2$, the degradation matrix $\mathbf{H}_2$ is equal to $\mathbf{H}_2^x \otimes \mathbf{H}_2^y$, where $\mathbf{H}_2^x$ is an $M_1 \times M_1$ tridiagonal matrix given by

$$\mathbf{H}_2^x = \frac{1}{2} \begin{pmatrix} \frac{3}{2} & \frac{1}{2} & & & \\ \frac{1}{2} & 1 & \frac{1}{2} & & \\ & \ddots & \ddots & \ddots & \\ & & \frac{1}{2} & 1 & \frac{1}{2} \\ & & & \frac{1}{2} & \frac{3}{2} \end{pmatrix} = \frac{1}{2} \begin{pmatrix} 1 & \frac{1}{2} & & & \\ \frac{1}{2} & 1 & \frac{1}{2} & & \\ & \ddots & \ddots & \ddots & \\ & & \frac{1}{2} & 1 & \frac{1}{2} \\ & & & \frac{1}{2} & 1 \end{pmatrix} + \frac{1}{2} \begin{pmatrix} \frac{1}{2} & 0 & & & \\ 0 & 0 & 0 & & \\ & \ddots & \ddots & \ddots & \\ & & 0 & 0 & 0 \\ & & & 0 & \frac{1}{2} \end{pmatrix}$$

and $\mathbf{H}_2^y$ is an $M_2 \times M_2$ matrix with the same structure.

In this particular case, the eigenvalues of $\mathbf{H}_L = \mathbf{H}_L^x \otimes \mathbf{H}_L^y$ can be computed easily as the matrix can be diagonalized by the 2-dimensional cosine transform $\mathbf{C}_{M_1} \otimes \mathbf{C}_{M_2}$ [17]. We note that the (i, j)-th entry of an N-by-N discrete cosine transform matrix $\mathbf{C}_N$ is given by

$$\sqrt{\frac{2 - \delta_{i1}}{N}} \cos \left(\frac{(i-1)(2j-1)\pi}{2N} \right)$$

and δ_{ij} is the Kronecker delta.

Lemma 1 *[17, Theorem 1] Under the Neumann boundary condition, the eigenvalues of $\mathbf{H}_L$ are given by*

$$\lambda_{(i-1)M_2+j}(\mathbf{H}_L) = \left(\frac{4}{L}\right)^2 \cos^2\left(\frac{(i-1)\pi}{2M_1}\right) \cos^2\left(\frac{(j-1)\pi}{2M_2}\right) p_L\left(\frac{(i-1)\pi}{M_1}\right) p_L\left(\frac{(j-1)\pi}{M_2}\right)$$

(11)

for $1 \leq i \leq M_1, 1 \leq j \leq M_2$. Here

$$p_L\left(\frac{(i-1)\pi}{M_1}\right) = \begin{cases} \sum_{k=1}^{L/4} \cos\left(\frac{(i-1)(2k-1)\pi}{M_1}\right), & L = 4l \text{ for some positive integer } l, \\ \frac{1}{2} + \sum_{k=1}^{(L-2)/4} \cos\left(\frac{(i-1)2k\pi}{M_1}\right), & \text{otherwise.} \end{cases}$$

In particular, by choosing $i = M_1$ with $j = M_2$ and $i = j = 1$, we have

$$0 \leq \lambda_{\min}(\mathbf{H}_L) \leq O\left(\frac{1}{M_1^2 M_2^2}\right) \quad \text{and} \quad \lambda_{\max}(\mathbf{H}_L) = 1.$$

(12)

In practical applications [8, 9], the within-channel degradation is always stronger than the cross-channel degradation, i.e.,

$$w_{ii} > w_{ij}, \quad \text{for} \quad j \neq i, \quad \text{and} \quad i \in \{r, g, b\}.$$

(13)

Under this assumption and using (6), we can prove that $\mathbf{W}$ is nonsingular.

Lemma 2 *Let $\mathbf{W}$ be a matrix with entries satisfying (6) and (13). Then $\mathbf{W}$ is nonsingular. Moreover, we have*

$$0 < \delta = \lambda_{\min}\{\mathbf{W}^t\mathbf{W}\} \leq \lambda_{\max}\{\mathbf{W}^t\mathbf{W}\} \leq 2,$$

(14)

where δ is a positive constant independent of M_1 and M_2.

Proof: By (6), it is easy to show that 1 is an eigenvalue of $\mathbf{W}$ with corresponding eigenvector $[1, 1, 1]^t$. Since the coefficients of the characteristic polynomial of $\mathbf{W}$ are real, the other two eigenvalues of $\mathbf{W}$ are in a conjugate pair. Suppose that $\mathbf{W}$ is a singular matrix, then $\mathbf{W}$ must be a rank one matrix, i.e.,

$$\mathbf{W} = \begin{pmatrix} u_1 \\ u_2 \\ u_3 \end{pmatrix} \cdot \begin{pmatrix} v_1 & v_2 & v_3 \end{pmatrix},$$

for some u_i, v_i. By (6), we can choose all $u_i, v_i \geq 0$. Also by (6), we have

$$u_1(v_1 + v_2 + v_3) = u_2(v_1 + v_2 + v_3) = u_3(v_1 + v_2 + v_3) = 1$$

or $u_1 = u_2 = u_3 = 1/(v_1 + v_2 + v_3)$. It implies that

$$w_{ij} = \frac{v_j}{v_1 + v_2 + v_3}.$$

6

However, this contradicts assumption (13) and hence $\mathbf{W}$ is nonsingular. In particular, we have the first inequality in (14). Since all the entries w_{ij} of $\mathbf{W}$ are independent of M_1 and M_2, we see that δ is also independent of M_1 and M_2. By (6) and (13), we have $\|\mathbf{W}\|_1 \leq 2$ and $\|\mathbf{W}\|_\infty = 1$. It follows that $\|\mathbf{W}\|_2^2 \leq \|\mathbf{W}\|_1 \|\mathbf{W}\|_\infty \leq 2$. $\quad\square$

Combining Lemmas 1 and 2 and using the tensor product structure (10) of $\mathbf{A}_L$, we get its condition number.

Theorem 1 *Let $\mathbf{W}$ be a matrix with entries satisfying (6) and (13). Under the Neumann boundary condition, if $\mathbf{H}_L$ is nonsingular, then the condition number $\kappa(\mathbf{A}_L)$ of $\mathbf{A}_L$ satisfies*

$$\kappa(\mathbf{A}_L) \geq O(M_1^2 M_2^2).$$

Proof: We first note that $\mathbf{H}_L$ is symmetric and

$$\|\mathbf{A}_L\|_2^2 = \lambda_{\max}(\mathbf{W}^t \mathbf{W} \otimes \mathbf{H}_L^t \mathbf{H}_L) = \lambda_{\max}(\mathbf{W}^t \mathbf{W}) \cdot \lambda_{\max}(\mathbf{H}_L^t \mathbf{H}_L) \geq \delta,$$

where the last inequality follows from (14) and (12). Again by (14) and (12),

$$\|\mathbf{A}_L^{-1}\|_2^2 = \frac{1}{\lambda_{\min}(\mathbf{W}^t \mathbf{W} \otimes \mathbf{H}_L^t \mathbf{H}_L)} = \frac{1}{\lambda_{\min}(\mathbf{W}^t \mathbf{W}) \cdot \lambda_{\min}(\mathbf{H}_L^t \mathbf{H}_L)} \geq \frac{1}{\delta} O(M_1^4 M_2^4). \quad\square$$

According to Theorem 1, $\mathbf{A}_L$ can be very ill-conditioned. In fact, some of them can be singular. For example, when $L = 4$ and $M_1 = M_2 = 64$, $\lambda_{33}(\mathbf{H}_L) = 0$. By continuity arguments, $\mathbf{A}_L(\epsilon)$ will still be ill-conditioned if the displacement errors are small. Therefore, a regularization procedure should be imposed to obtain a reasonable estimate of the original image.

2.3 Regularization

In the case of grey-level image reconstruction, the regularization operator only needs to enforce the spatial smoothness of the image. The most usual form of this operator is the discrete version of the 2-dimensional Laplacian. However, in color image reconstruction, in addition to the within-channel spatial smoothness, the cross-channel smoothness must also be enforced. One may incorporate the 3-dimensional discrete Laplacian here. However, color planes are highly correlated and this operator may fail to capture the cross-channel similarities.

In [8], Galatsanos et al. have proposed the following weighted discrete Laplacian matrix $\mathbf{R}$ as the regularization matrix:

$$\begin{aligned}[\mathbf{R}\mathbf{f}]_{r,j,k} \ = \ & 6[\mathbf{f}^{(r)}]_{j,k} - [\mathbf{f}^{(r)}]_{j-1,k} - [\mathbf{f}^{(r)}]_{j+1,k} - [\mathbf{f}^{(r)}]_{j,k-1} - [\mathbf{f}^{(r)}]_{j,k+1} - \\ & \frac{\|\tilde{\mathbf{f}}^{(r)}\|_2}{\|\tilde{\mathbf{f}}^{(g)}\|_2}[\mathbf{f}^{(g)}]_{j,k} - \frac{\|\tilde{\mathbf{f}}^{(r)}\|_2}{\|\tilde{\mathbf{f}}^{(b)}\|_2}[\mathbf{f}^{(b)}]_{j,k},\end{aligned}$$

$$[\mathbf{Rf}]_{g,j,k} = 6[\mathbf{f}^{(g)}]_{j,k} - [\mathbf{f}^{(g)}]_{j-1,k} - [\mathbf{f}^{(g)}]_{j+1,k} - [\mathbf{f}^{(g)}]_{j,k-1} - [\mathbf{f}^{(g)}]_{j,k+1} -$$
$$\frac{||\tilde{\mathbf{f}}^{(g)}||_2}{||\tilde{\mathbf{f}}^{(r)}||_2}[\mathbf{f}^{(r)}]_{j,k} - \frac{||\tilde{\mathbf{f}}^{(g)}||_2}{||\tilde{\mathbf{f}}^{(b)}||_2}[\mathbf{f}^{(b)}]_{j,k},$$

and

$$[\mathbf{Rf}]_{b,j,k} = 6[\mathbf{f}^{(b)}]_{j,k} - [\mathbf{f}^{(b)}]_{j-1,k} - [\mathbf{f}^{(b)}]_{j+1,k} - [\mathbf{f}^{(b)}]_{j,k-1} - [\mathbf{f}^{(b)}]_{j,k+1} -$$
$$\frac{||\tilde{\mathbf{f}}^{(b)}||_2}{||\tilde{\mathbf{f}}^{(g)}||_2}[\mathbf{f}^{(g)}]_{j,k} - \frac{||\tilde{\mathbf{f}}^{(b)}||_2}{||\tilde{\mathbf{f}}^{(r)}||_2}[\mathbf{f}^{(r)}]_{j,k},$$

for $1 \leq j \leq M_1$ and $1 \leq k \leq M_2$. Here $||\tilde{\mathbf{f}}^{(r)}||_2$, $||\tilde{\mathbf{f}}^{(g)}||_2$ and $||\tilde{\mathbf{f}}^{(b)}||_2$ are the estimates of the $||\mathbf{f}^{(r)}||_2$, $||\mathbf{f}^{(g)}||_2$ and $||\mathbf{f}^{(b)}||_2$ respectively and are assumed to be nonzero. The cross-channel weights of this regularization matrix capture the changes of reflectivity across the channels.

To sum up, the regularization matrix $\mathbf{R}$ is given by

$$\mathbf{R} = \begin{pmatrix} 2\mathbf{I} + \mathbf{L} & -\frac{||\tilde{\mathbf{f}}^{(r)}||_2}{||\tilde{\mathbf{f}}^{(g)}||_2}\mathbf{I} & -\frac{||\tilde{\mathbf{f}}^{(r)}||_2}{||\tilde{\mathbf{f}}^{(b)}||_2}\mathbf{I} \\ -\frac{||\tilde{\mathbf{f}}^{(g)}||_2}{||\tilde{\mathbf{f}}^{(r)}||_2}\mathbf{I} & 2\mathbf{I} + \mathbf{L} & -\frac{||\tilde{\mathbf{f}}^{(g)}||_2}{||\tilde{\mathbf{f}}^{(b)}||_2}\mathbf{I} \\ -\frac{||\tilde{\mathbf{f}}^{(b)}||_2}{||\tilde{\mathbf{f}}^{(r)}||_2}\mathbf{I} & -\frac{||\tilde{\mathbf{f}}^{(b)}||_2}{||\tilde{\mathbf{f}}^{(g)}||_2}\mathbf{I} & 2\mathbf{I} + \mathbf{L} \end{pmatrix} = \mathbf{S} \otimes \mathbf{I} + \mathbf{I} \otimes \mathbf{L}, \tag{15}$$

where $\mathbf{L}$ is the 2-dimensional discrete Laplacian matrix with the Neumann boundary condition, and

$$\mathbf{S} = \begin{pmatrix} 2 & -\frac{||\tilde{\mathbf{f}}^{(r)}||_2}{||\tilde{\mathbf{f}}^{(g)}||_2} & -\frac{||\tilde{\mathbf{f}}^{(r)}||_2}{||\tilde{\mathbf{f}}^{(b)}||_2} \\ -\frac{||\tilde{\mathbf{f}}^{(g)}||_2}{||\tilde{\mathbf{f}}^{(r)}||_2} & 2 & -\frac{||\tilde{\mathbf{f}}^{(g)}||_2}{||\tilde{\mathbf{f}}^{(b)}||_2} \\ -\frac{||\tilde{\mathbf{f}}^{(b)}||_2}{||\tilde{\mathbf{f}}^{(r)}||_2} & -\frac{||\tilde{\mathbf{f}}^{(b)}||_2}{||\tilde{\mathbf{f}}^{(g)}||_2} & 2 \end{pmatrix}. \tag{16}$$

We note that $\mathbf{L}$ can be diagonalized by the 2-dimensional cosine transform matrix $\mathbf{C}_{M_1} \otimes \mathbf{C}_{M_2}$ [4].

Using Tikhonov regularization in (3), our discretization problem becomes:

$$(\mathbf{A}_L(\epsilon)^t \Upsilon \mathbf{A}_L(\epsilon) + \mathbf{R}^t \mathbf{R})\mathbf{f} = \mathbf{A}_L(\epsilon)^t \Upsilon \mathbf{g}, \tag{17}$$

where $\mathbf{A}_L(\epsilon)$ is given in (10),

$$\Upsilon = \begin{pmatrix} \alpha_r \mathbf{I} & \mathbf{0} & \mathbf{0} \\ \mathbf{0} & \alpha_g \mathbf{I} & \mathbf{0} \\ \mathbf{0} & \mathbf{0} & \alpha_b \mathbf{I} \end{pmatrix} = \begin{pmatrix} \alpha_r & 0 & 0 \\ 0 & \alpha_g & 0 \\ 0 & 0 & \alpha_b \end{pmatrix} \otimes \mathbf{I} \equiv \Omega \otimes \mathbf{I},$$

and α_r, α_g and α_b are the regularization parameters which are assumed to be positive scalars.

Next we show that the regularized system (17) is well-conditioned. We begin with the case where there is no displacement error, i.e., $\epsilon^x_{\ell_1,\ell_2} = \epsilon^y_{\ell_1,\ell_2} = 0$. In that case,

$$\mathbf{A}_L^t \Upsilon \mathbf{A}_L + \mathbf{R}^t \mathbf{R} = \mathbf{W}\Omega\mathbf{W} \otimes \mathbf{H}_L^t \mathbf{H}_L + (\mathbf{S} \otimes \mathbf{I} + \mathbf{I} \otimes \mathbf{L})^t (\mathbf{S} \otimes \mathbf{I} + \mathbf{I} \otimes \mathbf{L}). \tag{18}$$

8

Theorem 2 *Let* $\mathbf{W}$ *be a matrix with entries satisfying (6) and (13). Then there exists a positive scalar* γ*, independent of* M_1 *and* M_2*, such that*

$$\lambda_{\min}\{\mathbf{A}_L^t \Upsilon \mathbf{A}_L + \mathbf{R}^t \mathbf{R}\} \geq \gamma > 0. \tag{19}$$

Proof: Under the Neumann boundary condition, the matrices $\mathbf{H}_L$ and $\mathbf{L}$ are symmetric and can be diagonalized by $\mathbf{C}_{M_1} \otimes \mathbf{C}_{M_2}$. From (18), it therefore suffices to consider the smallest eigenvalue of the matrix

$$\mathbf{W}^t \Omega \mathbf{W} \otimes \Lambda^2 + (\mathbf{S} \otimes \mathbf{I} + \mathbf{I} \otimes \Sigma)^t (\mathbf{S} \otimes \mathbf{I} + \mathbf{I} \otimes \Sigma) \tag{20}$$

where Λ and Σ are diagonal matrices with diagonal entries given by the eigenvalues of $\mathbf{H}_L$ and $\mathbf{L}$ respectively. More precisely, the diagonal entries Λ_{ij} of Λ are given in (11) and the diagonal entries of Σ are given by

$$\lambda_{(i-1)M_2+j}(\mathbf{L}) \equiv \Sigma_{ij} = 4\sin^2\left(\frac{(i-1)\pi}{2M_1}\right) + 4\sin^2\left(\frac{(j-1)\pi}{2M_2}\right), \tag{21}$$

for $1 \leq i \leq M_1$ and $1 \leq j \leq M_2$.

By permutation, we see that the eigenvalues of the matrix in (20) are the same as the eigenvalues of

$$\mathbf{B} \equiv \Lambda^2 \otimes \mathbf{W}^t \Omega \mathbf{W} + (\mathbf{I} \otimes \mathbf{S} + \Sigma \otimes \mathbf{I})^t (\mathbf{I} \otimes \mathbf{S} + \Sigma \otimes \mathbf{I}), \tag{22}$$

which is a block-diagonal matrix, i.e., all off-diagonal blocks are zero. It therefore suffices to estimate the smallest eigenvalues of the main diagonal blocks of $\mathbf{B}$. For $1 \leq i \leq M_1$, $1 \leq j \leq M_2$, the $((i-1)M_2+j, (i-1)M_2+j)$-th main diagonal block of $\mathbf{B}$ is equal to

$$\mathbf{B}_{ij} \equiv \Lambda_{ij}^2 \cdot \mathbf{W}^t \Omega \mathbf{W} + (\mathbf{S} + \Sigma_{ij}\mathbf{I})^t (\mathbf{S} + \Sigma_{ij}\mathbf{I}),$$

where Λ_{ij} is given by the expression in (11) and Σ_{ij} by (21). Since $\lambda_{\min}(\mathbf{X} + \mathbf{Y}) \geq \lambda_{\min}(\mathbf{X}) + \lambda_{\min}(\mathbf{Y})$ for any Hermitian matrices $\mathbf{X}$ and $\mathbf{Y}$ (see [10, Corollary 8.1.3, p.411]), we have

$$\lambda_{\min}(\mathbf{B}_{ij}) \geq \Lambda_{ij}^2 \lambda_{\min}(\mathbf{W}^t \Omega \mathbf{W}) + \lambda_{\min}\{(\mathbf{S} + \Sigma_{ij}\mathbf{I})^t (\mathbf{S} + \Sigma_{ij}\mathbf{I})\}.$$

By (14),

$$\lambda_{\min}(\mathbf{W}^t \Omega \mathbf{W}) \geq \min\{\alpha_r, \alpha_g, \alpha_b\} \cdot \lambda_{\min}(\mathbf{W}^t \mathbf{W}) = \delta \min\{\alpha_r, \alpha_g, \alpha_b\} \equiv \delta_0 > 0, \tag{23}$$

where δ_0 is a positive constant independent of M_1 and M_2. Hence

$$\lambda_{\min}(\mathbf{B}_{ij}) \geq \delta_0 \Lambda_{ij}^2 + \lambda_{\min}\{(\mathbf{S} + \Sigma_{ij}\mathbf{I})^t (\mathbf{S} + \Sigma_{ij}\mathbf{I})\}. \tag{24}$$

In view of (11) and (21), we define for simplicity

$$\chi(x, y) = \delta_0 \left(\frac{4}{L}\right)^4 \cos^4 x \cos^4 y \cdot p_L^2(2x) \, p_L^2(2y), \tag{25}$$

9

$$\phi(x, y) = 4 \sin^2 x + 4 \sin^2 y, \tag{26}$$

and

$$\psi(x, y) = \lambda_{\min} \left\{ (\mathbf{S} + \phi(x,y)\mathbf{I})^t (\mathbf{S} + \phi(x,y)\mathbf{I}) \right\}. \tag{27}$$

With these notations, (24) becomes

$$\lambda_{\min}(\mathbf{B}_{ij}) \geq \chi \left(\frac{(i-1)\pi}{2M_1}, \frac{(j-1)\pi}{2M_2} \right) + \psi \left(\frac{(i-1)\pi}{2M_1}, \frac{(j-1)\pi}{2M_2} \right), \tag{28}$$

with $1 \leq i \leq M_1, 1 \leq j \leq M_2$. To complete the proof, we now show that $\chi(x,y) + \psi(x,y) > 0$ for all $(x, y) \in [0, \pi/2]^2$.

From (16), it is easy to check that the eigenvalues of $\mathbf{S}$ are 0, 3 and 3 and their corresponding eigenvectors are

$$\left[\frac{||\tilde{\mathbf{f}}^{(r)}||_2}{||\tilde{\mathbf{f}}^{(b)}||_2}, \frac{||\tilde{\mathbf{f}}^{(g)}||_2}{||\tilde{\mathbf{f}}^{(b)}||_2}, 1 \right]^t, \quad \left[-\frac{||\tilde{\mathbf{f}}^{(r)}||_2}{||\tilde{\mathbf{f}}^{(b)}||_2}, 1, 0 \right]^t \quad \text{and} \quad \left[-\frac{||\tilde{\mathbf{f}}^{(r)}||_2}{||\tilde{\mathbf{f}}^{(g)}||_2}, 0, 1 \right]^t$$

respectively. Therefore, in view of definition (26), for all $(x, y) \in [0, \pi/2]^2$, the matrix $\mathbf{S} + \phi(x,y)\mathbf{I}$ is nonsingular except when $x = y = 0$. In particular, by definition (27), $\psi(x, y) > 0$ for all $(x, y) \in [0, \pi/2]^2$ except at $x = y = 0$. Moreover, since the entries $||\tilde{\mathbf{f}}^{(r)}||_2$, $||\tilde{\mathbf{f}}^{(g)}||_2$ and $||\tilde{\mathbf{f}}^{(b)}||_2$ of $\mathbf{S}$ are constants independent on M_1 and M_2, $\psi(x, y)$ depends only on x, y, $||\tilde{\mathbf{f}}^{(r)}||_2$, $||\tilde{\mathbf{f}}^{(g)}||_2$ and $||\tilde{\mathbf{f}}^{(b)}||_2$ but does not depend on M_1 and M_2.

On the other hand, since $\cos^4(x) p_L^2(2x) \geq 1/4$ at $x = 0$ and is nonnegative in $[0, \pi/2]$, by (25), $\chi(x, y) > 0$ at $x = y = 0$ and nonnegative in $[0, \pi/2]^2$. Therefore there exists a positive scalar γ independent of M_1 and M_2 such that $\chi(x, y) + \psi(x, y) \geq \gamma > 0$ for all $(x, y) \in [0, \pi/2]^2$. It follows from (28) that $\lambda_{\min}(\mathbf{B}_{ij}) \geq \gamma > 0$ for all $1 \leq i \leq M_1$, $1 \leq j \leq M_2$. $\square$

When there are errors in the subpixel displacements, the regularized matrix is given by

$$\mathbf{A}_L(\epsilon)^t \Upsilon \mathbf{A}_L(\epsilon) + \mathbf{R}^t \mathbf{R} = \mathbf{W}^t \Omega \mathbf{W} \otimes \mathbf{H}_L(\epsilon)^t \mathbf{H}_L(\epsilon) + \mathbf{R}^t \mathbf{R}.$$

The following corollary states that when the errors are sufficiently small, the regularized matrix is also well-conditioned.

Corollary 1 *Let $\epsilon^* = \max_{0 \leq l_1, l_2 \leq L-1} \{|\epsilon_{l_1 l_2}^x|, |\epsilon_{l_1 l_2}^y|\}$ and $\mathbf{W}$ be a matrix with entries satisfying (6) and (13). If ϵ^* is sufficiently small, then the smallest eigenvalue of $\mathbf{W}^t \Omega \mathbf{W} \otimes \mathbf{H}_L(\epsilon)^t \mathbf{H}_L(\epsilon) + \mathbf{R}^t \mathbf{R}$ is uniformly bounded away from 0 by a positive constant independent of M_1 and M_2.*

Proof: We first claim that $\|\mathbf{H}_L(\epsilon)^t \mathbf{H}_L(\epsilon) - \mathbf{H}_L^t \mathbf{H}_L\|_2 \leq 16\epsilon^*$. From (9), every row or column of $\mathbf{H}_L(\epsilon)$ and $\mathbf{H}_L$ differ in at most $4L$ entries and each of these entries is bounded by ϵ^*/L. It follows that $\|\mathbf{H}_L(\epsilon) - \mathbf{H}_L\|_\infty \leq 4\epsilon^*$ and $\|\mathbf{H}_L(\epsilon) - \mathbf{H}_L\|_1 \leq 4\epsilon^*$. Hence

$$\|\mathbf{H}_L(\epsilon) - \mathbf{H}_L\|_2 \leq \{\|\mathbf{H}_L(\epsilon) - \mathbf{H}_L\|_\infty \|\mathbf{H}_L(\epsilon) - \mathbf{H}_L\|_1\}^{1/2} \leq 4\epsilon^*. \tag{29}$$

10

Thus $\|\mathbf{H}_L(\epsilon)\|_2 \leq \|\mathbf{H}_L\|_2 + 4\epsilon^*$. Hence by (12) and (4),

$$\|\mathbf{H}_L(\epsilon)\|_2 \leq 3. \tag{30}$$

Therefore,

$$
\begin{aligned}
\|\mathbf{H}_L(\epsilon)^t\mathbf{H}_L(\epsilon) - \mathbf{H}_L^t\mathbf{H}_L\|_2 &\leq \|\mathbf{H}_L(\epsilon)^t[\mathbf{H}_L(\epsilon) - \mathbf{H}_L]\|_2 + \|[\mathbf{H}_L(\epsilon)^t - \mathbf{H}_L^t]\mathbf{H}_L\|_2 \\
&\leq \|\mathbf{H}_L(\epsilon) - \mathbf{H}_L\|_2\{\|\mathbf{H}_L(\epsilon)\|_2 + \|\mathbf{H}_L\|_2\} \leq 16\epsilon^*, \tag{31}
\end{aligned}
$$

where the last inequality follows from (29), (30) and (12).

To complete the proof, we next show that $\|[\mathbf{W}^t\Omega\mathbf{W} \otimes \mathbf{H}_L(\epsilon)^t\mathbf{H}_L(\epsilon) + \mathbf{R}^t\mathbf{R}]^{-1}\|_2$ is bounded above by a constant independent of M_1 and M_2. Since $\lambda_{\min}(\mathbf{X}) + \lambda_{\min}(\mathbf{Y}) \leq \lambda_{\min}(\mathbf{X} + \mathbf{Y})$ for any Hermitian matrices $\mathbf{X}$ and $\mathbf{Y}$ (see [10, Corollary 8.1.3, p.411]), we have

$$
\begin{aligned}
&\|[\mathbf{W}^t\Omega\mathbf{W} \otimes \mathbf{H}_L(\epsilon)^t\mathbf{H}_L(\epsilon) + \mathbf{R}^t\mathbf{R}]^{-1}\|_2 \\
=\ & \frac{1}{\lambda_{\min}(\mathbf{W}^t\Omega\mathbf{W} \otimes \mathbf{H}_L(\epsilon)^t\mathbf{H}_L(\epsilon) + \mathbf{R}^t\mathbf{R})} \\
\leq\ & \frac{1}{\lambda_{\min}(\mathbf{W}^t\Omega\mathbf{W} \otimes \mathbf{H}_L^t\mathbf{H}_L + \mathbf{R}^t\mathbf{R}) + \lambda_{\min}((\mathbf{W}^t\Omega\mathbf{W}) \otimes [\mathbf{H}_L(\epsilon)^t\mathbf{H}_L(\epsilon) - \mathbf{H}_L^t\mathbf{H}_L])} \\
=\ & \frac{1}{\lambda_{\min}(\mathbf{W}^t\Omega\mathbf{W} \otimes \mathbf{H}_L^t\mathbf{H}_L + \mathbf{R}^t\mathbf{R}) + \lambda_{\min}(\mathbf{W}^t\Omega\mathbf{W}) \cdot \lambda_{\min}(\mathbf{H}_L(\epsilon)^t\mathbf{H}_L(\epsilon) - \mathbf{H}_L^t\mathbf{H}_L)} \\
\leq\ & \frac{1}{\lambda_{\min}(\mathbf{W}^t\Omega\mathbf{W} \otimes \mathbf{H}_L^t\mathbf{H}_L + \mathbf{R}^t\mathbf{R}) + \delta_0 \cdot \lambda_{\min}(\mathbf{H}_L(\epsilon)^t\mathbf{H}_L(\epsilon) - \mathbf{H}_L^t\mathbf{H}_L)},
\end{aligned}
$$

where the last inequality follows from (23). Note that by (19),

$$\lambda_{\min}(\mathbf{W}^t\Omega\mathbf{W} \otimes \mathbf{H}_L^t\mathbf{H}_L + \mathbf{R}^t\mathbf{R}) = \lambda_{\min}(\mathbf{A}_L^t\Upsilon\mathbf{A}_L + \mathbf{R}^t\mathbf{R}) \geq \gamma > 0.$$

Combining this with (31), we have

$$
\begin{aligned}
&\|[\mathbf{W}^t\Omega\mathbf{W} \otimes \mathbf{H}_L(\epsilon)^t\mathbf{H}_L(\epsilon) + \mathbf{R}^t\mathbf{R}]^{-1}\|_2 \\
\leq\ & \frac{1}{\lambda_{\min}(\mathbf{W}^t\Omega\mathbf{W} \otimes \mathbf{H}_L^t\mathbf{H}_L + \mathbf{R}^t\mathbf{R}) - \delta_0 \cdot \|\mathbf{H}_L(\epsilon)^t\mathbf{H}_L(\epsilon) - \mathbf{H}_L^t\mathbf{H}_L\|_2} \leq \frac{1}{\gamma - 16\delta_0\epsilon^*}.
\end{aligned}
$$

Since both γ and δ_0 are constants independent of M_1 and M_2, the collorary follows. $\quad\square$

Thus we see that the condition number of $\mathbf{A}_L(\epsilon)^t\Upsilon\mathbf{A}_L(\epsilon)$ is improved by the regularization.

3 Spatially Invariant Case

When there are no subpixel displacement errors, i.e., when all $\epsilon_{l_1,l_2}^x = \epsilon_{l_1,l_2}^y = 0$, we have to solve $(\mathbf{A}_L^t\Upsilon\mathbf{A}_L + \mathbf{R}^t\mathbf{R})\mathbf{f} = \mathbf{A}_L^t\Upsilon\mathbf{g}$ which according to (18) can be simplified to

$$(\mathbf{W}^t\Omega\mathbf{W} \otimes \mathbf{H}_L^t\mathbf{H}_L + \mathbf{R}^t\mathbf{R})\mathbf{f} = (\mathbf{W}^t\Omega \otimes \mathbf{H}_L^t)\mathbf{g}. \tag{32}$$

11

Recall that if we use the Neumann boundary condition for both $\mathbf{H}_L$ and $\mathbf{L}$, then both matrices can be diagonalized by discrete cosine transform matrices. From (18) and (20), we see that (32) is equivalent to

$$[\mathbf{W}^t\Omega\mathbf{W} \otimes \Lambda^2 + (\mathbf{S} \otimes \mathbf{I} + \mathbf{I} \otimes \Sigma)^t(\mathbf{S} \otimes \mathbf{I} + \mathbf{I} \otimes \Sigma)]\hat{\mathbf{f}} = (\mathbf{W}^t\Omega \otimes \Lambda)\hat{\mathbf{g}}, \tag{33}$$

where $\hat{\mathbf{f}} = (\mathbf{I} \otimes \mathbf{C}_{M_1} \otimes \mathbf{C}_{M_2})\mathbf{f}$ and $\hat{\mathbf{g}} = (\mathbf{I} \otimes \mathbf{C}_{M_1} \otimes \mathbf{C}_{M_2})\mathbf{g}$. The system in (33) is a block-diagonalized system of $M_1 M_2$ decoupled subsystems. The vector $\hat{\mathbf{f}}$ can be computed by solving a set of $M_1 M_2$ decoupled 3-by-3 matrix equations (cf. (22)). The total cost of solving the system is therefore of $O(M_1 M_2 \log M_1 M_2)$ operations.

4 Spatially Variant Case

When there are subpixel displacement errors, the matrix $\mathbf{H}_L(\epsilon)$ has the same banded structure as that of $\mathbf{H}_L$, but with some entries slightly perturbed. It is a near block-Toeplitz-Toeplitz-block matrix but it can no longer be diagonalized by the cosine transform matrix. Therefore we solve the linear system in (17) by the preconditioned conjugate gradient method. For an $M_1 \times M_1$ block matrix $\mathbf{H}_L(\epsilon)$ with the size of each block equal to $M_2 \times M_2$, the cosine transform preconditioner $c(\mathbf{H}_L(\epsilon))$ of $\mathbf{H}_L(\epsilon)$ is defined to be the matrix $(\mathbf{C}_{M_1} \otimes \mathbf{C}_{M_2})\Phi(\mathbf{C}_{M_1} \otimes \mathbf{C}_{M_2})$ that minimizes

$$\|(\mathbf{C}_{M_1} \otimes \mathbf{C}_{M_2})\Phi(\mathbf{C}_{M_1} \otimes \mathbf{C}_{M_2}) - \mathbf{H}_L(\epsilon)\|_F$$

over all diagonal matrices Φ, where $\| \cdot \|_F$ is the Frobenius norm, see [7]. Clearly, the cost of computing $c(\mathbf{H}_L(\epsilon))^{-1}\mathbf{y}$ for any vector $\mathbf{y}$ is $O(M_1 M_2 \log M_1 M_2)$ operations. Since $\mathbf{H}_L(\epsilon)$ in (9) is a banded matrix with $(2L-1)^2$ non-zero diagonals and is of size $M_1 M_2 \times M_1 M_2$, the cost of constructing $c(\mathbf{H}_L(\epsilon))$ is of $O(L^2 M_1 M_2)$ operations only, see [6].

We will employ the cosine transform preconditioner $c(\mathbf{H}_L(\epsilon))$ of $\mathbf{H}_L(\epsilon)$ in our preconditioner. Below we study the convergence rate of the conjugate gradient method for solving the preconditioned system

$$
\begin{aligned}
&[\mathbf{W}^t\Omega\mathbf{W} \otimes c(\mathbf{H}_L(\epsilon))^t c(\mathbf{H}_L(\epsilon)) + \mathbf{R}^t\mathbf{R}]^{-1}[\mathbf{W}^t\Omega\mathbf{W} \otimes \mathbf{H}_L(\epsilon)^t\mathbf{H}_L(\epsilon) + \mathbf{R}^t\mathbf{R}]\mathbf{f} \\
&= [\mathbf{W}^t\Omega \otimes \mathbf{H}_L(\epsilon)^t]\mathbf{g}.
\end{aligned} \tag{34}
$$

We prove that the spectra of the preconditioned normal system are clustered around 1 for sufficiently small subpixel displacement errors. Hence when the conjugate gradient method is applied to solving (34), we have fast convergence. Our numerical results in §5 show that the cosine transform preconditioners can indeed speed up the convergence of the method. We begin the proof with the following lemma.

Lemma 3 *Let* $\epsilon^* = \max_{0 \le l_1, l_2 \le L-1}\{|\epsilon^x_{l_1 l_2}|, |\epsilon^y_{l_1 l_2}|\}$ *and* $\mathbf{W}$ *be a matrix with entries satisfying (6) and (13). Then*

$$\|\mathbf{H}_L(\epsilon)^t\mathbf{H}_L(\epsilon) - c(\mathbf{H}_L(\epsilon))^t c(\mathbf{H}_L(\epsilon))\|_2 \le 48\epsilon^* \tag{35}$$

and

$$\|\mathbf{W}^t\Omega\mathbf{W} \otimes [\mathbf{H}_L(\epsilon)^t\mathbf{H}_L(\epsilon) - c(\mathbf{H}_L(\epsilon))^t c(\mathbf{H}_L(\epsilon))]\|_2 \le 96 \cdot \max\{\alpha_r, \alpha_g, \alpha_b\} \cdot \epsilon^*. \tag{36}$$

12

Proof: We note that

$$\|\mathbf{W}^t\Omega\mathbf{W} \otimes [\mathbf{H}_L(\epsilon)^t\mathbf{H}_L(\epsilon) - c(\mathbf{H}_L(\epsilon))^t c(\mathbf{H}_L(\epsilon))]\|_2$$

$$= \quad \|\mathbf{W}^t\Omega\mathbf{W}\|_2 \|\mathbf{H}_L(\epsilon)^t\mathbf{H}_L(\epsilon) - c(\mathbf{H}_L(\epsilon))^t c(\mathbf{H}_L(\epsilon))\|_2$$

$$\leq \quad \|\mathbf{W}^t\Omega\mathbf{W}\|_2 \left\{ \|\mathbf{H}_L(\epsilon)^t[\mathbf{H}_L(\epsilon) - c(\mathbf{H}_L(\epsilon))]\|_2 + \|[\mathbf{H}_L(\epsilon)^t - c(\mathbf{H}_L(\epsilon))^t] c(\mathbf{H}_L(\epsilon))\|_2 \right\}$$

$$\leq \quad \|\mathbf{W}^t\Omega\mathbf{W}\|_2 \|\mathbf{H}_L(\epsilon) - c(\mathbf{H}_L(\epsilon))\|_2 \{\|\mathbf{H}_L(\epsilon)\|_2 + \|c(\mathbf{H}_L(\epsilon))\|_2\}.$$

Recall that by (30), $\|\mathbf{H}_L(\epsilon)\|_2 \leq 3$. Since $\|c(\cdot)\|_2 \leq \|\cdot\|_2$ (see [2]), we have

$$\|c(\mathbf{H}_L(\epsilon))\|_2 \leq \|\mathbf{H}_L(\epsilon)\|_2 \leq 3.$$

Note that $c(\mathbf{H}_L) = \mathbf{H}_L$, we then have by (29),

$$\|\mathbf{H}_L(\epsilon) - c(\mathbf{H}_L(\epsilon))\|_2 \quad \leq \quad \|\mathbf{H}_L(\epsilon) - \mathbf{H}_L\|_2 + \|\mathbf{H}_L - c(\mathbf{H}_L(\epsilon))\|_2$$

$$= \quad \|\mathbf{H}_L(\epsilon) - \mathbf{H}_L\|_2 + \|c(\mathbf{H}_L - \mathbf{H}_L(\epsilon))\|_2$$

$$\leq \quad 2\|\mathbf{H}_L(\epsilon) - \mathbf{H}_L\|_2 \leq 8\epsilon^*.$$

Finally, by (14), $\|\mathbf{W}^t\Omega\mathbf{W}\|_2 \leq \max\{\alpha_r, \alpha_g, \alpha_b\} \cdot \|\mathbf{W}^t\mathbf{W}\|_2 \leq 2 \cdot \max\{\alpha_r, \alpha_g, \alpha_b\}$. $\quad\square$

Theorem 3 *Let $\epsilon^* = \max_{0 \leq l_1, l_2 \leq L-1}\{|\epsilon^x_{l_1 l_2}|, |\epsilon^y_{l_1 l_2}|\}$ and $\mathbf{W}$ be a matrix with entries satisfying (6) and (13). If ϵ^* is sufficiently small, then the spectra of the preconditioned matrices*

$$[\mathbf{W}^t\Omega\mathbf{W} \otimes c(\mathbf{H}_L(\epsilon))^t c(\mathbf{H}_L(\epsilon)) + \mathbf{R}^t\mathbf{R}]^{-1}[\mathbf{W}^t\Omega\mathbf{W} \otimes \mathbf{H}_L(\epsilon)^t\mathbf{H}_L(\epsilon) + \mathbf{R}^t\mathbf{R}]$$

are clustered around 1 and their smallest eigenvalues are uniformly bounded away from 0 by a positive constant independent of M_1 and M_2.

Proof: We note that

$$[\mathbf{W}^t\Omega\mathbf{W} \otimes c(\mathbf{H}_L(\epsilon))^t c(\mathbf{H}_L(\epsilon)) + \mathbf{R}^t\mathbf{R}]^{-1}[\mathbf{W}^t\Omega\mathbf{W} \otimes \mathbf{H}_L(\epsilon)^t\mathbf{H}_L(\epsilon) + \mathbf{R}^t\mathbf{R}]$$

$$= \quad \mathbf{I} + [\mathbf{W}^t\Omega\mathbf{W} \otimes c(\mathbf{H}_L(\epsilon))^t c(\mathbf{H}_L(\epsilon)) + \mathbf{R}^t\mathbf{R}]^{-1} \cdot$$

$$\cdot (\mathbf{W}^t\Omega\mathbf{W}) \otimes [\mathbf{H}_L(\epsilon)^t\mathbf{H}_L(\epsilon) - c(\mathbf{H}_L(\epsilon))^t c(\mathbf{H}_L(\epsilon))].$$

In view of (36), it suffices to show that $\|[\mathbf{W}^t\Omega\mathbf{W} \otimes c(\mathbf{H}_L(\epsilon))^t c(\mathbf{H}_L(\epsilon)) + \mathbf{R}^t\mathbf{R}]^{-1}\|_2$ is bounded above by a constant independent of M_1 and M_2. Then we note that

$$\|[\mathbf{W}^t\Omega\mathbf{W} \otimes c(\mathbf{H}_L(\epsilon))^t c(\mathbf{H}_L(\epsilon)) + \mathbf{R}^t\mathbf{R}]^{-1}\|_2$$

$$= \quad \frac{1}{\lambda_{\min}(\mathbf{W}^t\Omega\mathbf{W} \otimes c(\mathbf{H}_L(\epsilon))^t c(\mathbf{H}_L(\epsilon)) + \mathbf{R}^t\mathbf{R})}$$

$$\leq \quad \frac{1}{\lambda_{\min}(\mathbf{W}^t\Omega\mathbf{W} \otimes \mathbf{H}_L^t\mathbf{H}_L + \mathbf{R}^t\mathbf{R}) + \lambda_{\min}\{\mathbf{W}^t\Omega\mathbf{W} \otimes [c(\mathbf{H}_L(\epsilon))^t c(\mathbf{H}_L(\epsilon)) - \mathbf{H}_L^t\mathbf{H}_L)]\}}$$

$$\leq \quad \frac{1}{\lambda_{\min}(\mathbf{W}^t\Omega\mathbf{W} \otimes \mathbf{H}_L^t\mathbf{H}_L + \mathbf{R}^t\mathbf{R}) + \delta_0\lambda_{\min}[c(\mathbf{H}_L(\epsilon))^t c(\mathbf{H}_L(\epsilon)) - \mathbf{H}_L^t\mathbf{H}_L)]},$$

where δ_0 is given in (23). Hence

$$\|[\mathbf{W}^t\Omega\mathbf{W} \otimes c(\mathbf{H}_L(\epsilon))^t c(\mathbf{H}_L(\epsilon)) + \mathbf{R}^t\mathbf{R}]^{-1}\|_2$$
$$\leq \frac{1}{\lambda_{\min}(\mathbf{W}^t\Omega\mathbf{W} \otimes \mathbf{H}_L^t\mathbf{H}_L + \mathbf{R}^t\mathbf{R}) - \delta_0\|c(\mathbf{H}_L(\epsilon))^t c(\mathbf{H}_L(\epsilon)) - \mathbf{H}_L^t\mathbf{H}_L\|_2} \leq \frac{1}{\gamma - 48\delta_0\epsilon^*}$$

where the last inequality follows from (19) and (35). Since γ and δ_0 are positive constants independent of M_1 and M_2, the last expression is therefore bounded above by a positive constant independent of M_1 and M_2 for sufficiently small ϵ^*. $\square$

Using standard convergence analysis of the conjugate gradient method, see for instance [10, p.525], we conclude that the conjugate gradient method applied to the preconditioned system (34) will converge superlinearly for sufficiently small displacement errors. Since $\mathbf{H}_L(\epsilon)$ has only $(2L - 1)^2$ non-zero diagonals, the matrix-vector product $\mathbf{A}_L(\epsilon)\mathbf{x}$ can be done in $O(L^2 M_1 M_2)$. Thus the cost per each PCG iteration is $O(M_1 M_2 \log M_1 M_2 + L^2 M_1 M_2)$ operations, see [10, p.529]. Hence the total cost for finding the high resolution image vector is of $O(M_1 M_2 \log M_1 M_2 + L^2 M_1 M_2)$ operations.

5 Numerical Examples

In this section, we illustrate the effectiveness of using cosine transform preconditioners for solving high resolution color image reconstruction problems. The 128×128 original image is shown in Figure 1. The conjugate gradient method is employed to solving the preconditioned system (34). The cross-channel weights for $\mathbf{R}$ (see (15)) are computed from the observed high-resolution image, i.e.,

$$\|\tilde{\mathbf{f}}^{(i)}\|_2 = \|\mathbf{g}^{(i)}\|_2, \quad i \in \{r, g, b\}.$$

We tried the following two different degradation matrices to degrade the original color image

$$(i) \quad \begin{pmatrix} 0.8 & 0.1 & 0.1 \\ 0.1 & 0.8 & 0.1 \\ 0.1 & 0.1 & 0.8 \end{pmatrix} \otimes \mathbf{H}_L(\epsilon) \quad \text{and} \quad (ii) \quad \begin{pmatrix} 0.5 & 0.3 & 0.2 \\ 0.2 & 0.5 & 0.3 \\ 0.3 & 0.2 & 0.5 \end{pmatrix} \otimes \mathbf{H}_L(\epsilon). \quad (37)$$

We note that the interdependency between cross-channels of the first degradation matrix is higher than that of the second degradation matrix. Gaussian white noises with signal-to-noise ratio of 30 dB were added to each degraded image plane.

In the tests, we used the same regularization parameter for each channel, i.e., $\alpha_r = \alpha_g = \alpha_b = \alpha$. The initial guess was the zero vector and the stopping criteria was $\|\mathbf{r}^{(j)}\|_2/\|\mathbf{r}^{(0)}\|_2 < 10^{-6}$, where $\mathbf{r}^{(j)}$ is the normal equations residual after j iterations. Tables 1–4 show the numbers of iterations required for convergence for $L = 2$ and 4, i.e., the number of sensor array used is 2×2 and 4×4 respectively. In the tables, "cos", "cir" or "no" signify that the cosine transform preconditioner, the level-2 circulant preconditioner [7] or no preconditioner is used respectively.

We see from the tables that for both degradation matrices, the cosine transform preconditioner converges much faster than the circulant preconditioners for different M, α and $\epsilon_{l_1 l_2}^{x,y}$, where

$M(= M_1 = M_2)$ is the size of the reconstructed image and $\epsilon_{l_1 l_2}^{x,y}$ are the subpixel displacement errors. Also the convergence rate is independent of M for fixed α or $\epsilon_{l_1 l_2}^{x,y}$.

α	2×10^2			2×10^3			2×10^4		
M	cos	cir	no	cos	cir	no	cos	cir	no
32	6	16	19	8	38	47	12	95	122
64	6	16	19	8	38	46	11	97	121
128	6	15	19	7	37	47	12	97	121
256	6	15	19	7	38	47	10	98	121

Table 1a: Number of iterations for degradation matrix (i) with $L = 2$ and $\epsilon_{l_1 l_2}^x = \epsilon_{l_1 l_2}^y = 0.1$.

α	2×10^2			2×10^3			2×10^4		
M	cos	cir	no	cos	cir	no	cos	cir	no
32	9	17	20	13	40	48	24	95	120
64	9	16	20	13	39	48	21	99	122
128	8	16	19	12	39	47	23	99	121
256	8	16	20	11	39	48	21	100	122

Table 1b: Number of iterations for degradation matrix (i) with $L = 2$ and $\epsilon_{l_1 l_2}^x = \epsilon_{l_1 l_2}^y = 0.2$.

α	2×10^2			2×10^3			2×10^4		
M	cos	cir	no	cos	cir	no	cos	cir	no
32	12	18	21	20	42	50	42	95	117
64	11	17	20	18	42	49	38	102	126
128	11	17	20	18	41	48	39	101	123
256	11	17	20	17	41	48	37	102	124

Table 1c. Number of iterations for degradation matrix (i) with $L = 2$ and $\epsilon_{l_1 l_2}^x = \epsilon_{l_1 l_2}^y = 0.3$.

Next we have shown the 128×128 images reconstructed from four 64×64 low resolution images from a 2×2 sensor array and from sixteen 32×32 low resolution images fron a 4×4 sensor array. The first degradation matrix in (37) is used here. Two low resolution images are shown in Figure 2 (left) and Figure 5 (left). The observed high resolution images $\mathbf{g}$ are also shown in Figure 2 (right) and Figure 5 (right). Figures 3 and 6 give the reconstructed images under the Neumann boundary condition whereas Figures 4 and 7 are the reconstructed images for periodic and zero boundary conditions.

In all cases, the optimal regularization parameter α is chosen such that it minimizes the relative error. Here the relative error of the reconstructed image $\mathbf{f}_c$ to the original image $\mathbf{f}$ is defined as:

$$\sum_{i \in \{r,g,b\}} \frac{\|\mathbf{f}^{(i)} - \mathbf{f}_c^{(i)}\|_2}{\|\mathbf{f}^{(i)}\|_2}.$$

α	2×10^2			2×10^3			2×10^4		
M	cos	cir	no	cos	cir	no	cos	cir	no
32	6	16	21	8	39	48	12	95	121
64	6	16	21	8	38	47	11	99	122
128	6	15	20	7	38	46	12	97	121
256	6	15	20	7	38	47	10	98	122

Table 2a. Number of iterations for degradation matrix (ii) with $L = 2$ and $\epsilon^x_{l_1 l_2} = \epsilon^y_{l_1 l_2} = 0.1$.

α	2×10^2			2×10^3			2×10^4		
M	cos	cir	no	cos	cir	no	cos	cir	no
32	9	17	20	13	40	49	24	96	120
64	9	17	20	13	40	48	21	100	122
128	8	16	20	12	39	47	23	99	121
256	8	16	20	11	39	48	21	99	122

Table 2b. Number of iterations for degradation matrix (ii) with $L = 2$ and $\epsilon^x_{l_1 l_2} = \epsilon^y_{l_1 l_2} = 0.2$.

α	2×10^2			2×10^3			2×10^4		
M	cos	cir	no	cos	cir	no	cos	cir	no
32	12	18	21	20	43	51	42	94	117
64	11	17	21	18	42	50	38	102	127
128	11	17	20	17	41	48	39	101	123
256	11	17	20	17	41	48	37	103	124

Table 2c. Number of iterations for degradation matrix (ii) with $L = 2$ and $\epsilon^x_{l_1 l_2} = \epsilon^y_{l_1 l_2} = 0.3$.

Table 5 lists the optimal regularization parameters and the corresponding relative errors of the reconstructed images. By comparing Figures 3–4 and 6–7, it is clear that the details in the image are much better reconstructed under the Neumann boundary condition than that under the zero and periodic boundary conditions. Moreover, the boundary artifacts under the Neumann boundary condition are less prominent too.

References

[1] M. Banham and A. Katsaggelos, *Digital image restoration*, IEEE Signal Processing Magazine, 14 (1997), pp. 24–41.

[2] E. Boman, *Fast Algorithms for Toeplitz Equations*, PhD thesis, University of Connecticut, Storrs, CT, October 1993.

α	2×10^2			2×10^3			2×10^4		
M	cos	cir	no	cos	cir	no	cos	cir	no
32	5	27	34	7	55	64	11	107	130
64	5	28	34	7	64	79	10	147	161
128	5	25	33	7	64	81	10	169	181
256	5	23	33	6	60	81	10	167	211

Table 3a. Number of iterations for degradation matrix (i) with $L = 4$ and $\epsilon^x_{l_1 l_2} = \epsilon^y_{l_1 l_2} = 0.1$.

α	2×10^2			2×10^3			2×10^4		
M	cos	cir	no	cos	cir	no	cos	cir	no
32	7	26	34	11	56	66	20	109	134
64	7	29	35	11	66	81	20	151	162
128	7	25	33	10	66	82	19	166	182
256	6	24	33	10	59	82	19	171	209

Table 3b. Number of iterations for degradation matrix (i) with $L = 4$ and $\epsilon^x_{l_1 l_2} = \epsilon^y_{l_1 l_2} = 0.2$.

α	2×10^2			2×10^3			2×10^4		
M	cos	cir	no	cos	cir	no	cos	cir	no
32	9	27	35	16	57	69	31	115	135
64	9	29	35	15	67	81	31	159	161
128	8	26	34	15	67	83	31	172	181
256	8	25	33	14	61	83	30	170	211

Table 3c. Number of iterations for degradation matrix (i) with $L = 4$ and $\epsilon^x_{l_1 l_2} = \epsilon^y_{l_1 l_2} = 0.3$.

[3] N. Bose and K. Boo, *High-resolution image reconstruction with multisensors*, International Journal of Imaging Systems and Technology, 9 (1998), pp. 294–304.

[4] M. Buckley, *Fast computation of a discretized thin-plate smoothing spline for image data*, Biometrika, 81 (1994), pp. 247–258.

[5] R. Chan, T. Chan, M. Ng, W. Tang, and C. Wong, *Preconditioned iterative methods for high-resolution image reconstruction with multisensors*, Proceedings to the SPIE Symposium on Advanced Signal Processing: Algorithms, Architectures, and Implementations, Vol. 3461, San Diego CA, July, 1998, pp. 348–357, Ed: F. Luk.

[6] R. Chan, T. Chan, and C. Wong, *Cosine Transform Based Preconditioners for Total Variation Minimization Problems in Image Processing*, Iterative Methods in Linear Algebra, II, V3, IMACS Series in Computational and Applied Mathematics, Proceedings of the Second IMACS International Symposium on Iterative Methods in Linear Algebra, Bulgaria, June, 1995, pp. 311–329, Ed: S. Margenov and P. Vassilevski.

α	2×10^2			2×10^3			2×10^4		
M	cos	cir	no	cos	cir	no	cos	cir	no
32	5	26	34	7	46	64	11	90	129
64	5	28	34	7	63	80	10	131	159
128	5	24	33	7	61	82	10	152	183
256	5	22	33	6	58	81	10	162	209

Table 4a. Number of iterations for degradation matrix (ii) with $L = 4$ and $\epsilon^x_{l_1 l_2} = \epsilon^y_{l_1 l_2} = 0.1$.

α	2×10^2			2×10^3			2×10^4		
M	cos	cir	no	cos	cir	no	cos	cir	no
32	7	26	35	11	49	64	20	92	131
64	7	28	35	11	64	80	20	136	162
128	7	24	34	10	63	81	19	156	183
256	6	23	33	10	59	82	18	163	209

Table 4b. Number of iterations for degradation matrix (ii) with $L = 4$ and $\epsilon^x_{l_1 l_2} = \epsilon^y_{l_1 l_2} = 0.2$.

α	2×10^2			2×10^3			2×10^4		
M	cos	cir	no	cos	cir	no	cos	cir	no
32	9	27	35	16	49	68	31	98	134
64	9	29	35	15	64	81	31	142	162
128	8	25	34	14	63	84	30	160	181
256	8	25	33	14	59	84	29	169	211

Table 4c. Number of iterations for degradation matrix (ii) with $L = 4$ and $\epsilon^x_{l_1 l_2} = \epsilon^y_{l_1 l_2} = 0.3$.

[7] R. Chan and M. Ng, *Conjugate gradient method for Toeplitz system*, SIAM Review, 38 (1996), pp. 427–482.

[8] N. Galatsanos, A. Katsaggelosm, R. Chin, and A. Hillery, *Least Squares Restoration of Mulitchannel Images*, IEEE Trans. Signal Processing, 39 (1991), pp. 2222–2236.

[9] N. Galatsanos and R. Chin, *Restoration of Color Images by Multichannel Kalman Filtering*, IEEE Trans. Signal Processing, 39 (1991), pp. 2237–2252.

[10] G. Golub and C. Van Loan, *Matrix Computations*, 2rd ed., The Johns Hopkins University Press, 1993.

[11] B. Hunt and O. Kubler, *Karhunen-Loeve Multispectral Image Restoration, Part I: Theoey*, IEEE Trans. Acoust., Speech, Signal Processing, 32 (1984), pp. 592–600.

	Boundary Conditions					
	Neumann		Zero		Periodic	
	α	Error	α	Error	α	Error
2×2 sensor array	7×10^2	0.2724	1×10^2	0.5404	1×10^2	0.5381
4×4 sensor array	1.2×10^3	0.2003	1×10^2	0.2960	1×10^2	0.2958

Table 5: The optimal regularization parameters and their relative errors.

[12] E. Kaltenbacher and R. Hardie, *High resolution infrared image reconstruction using multiple, low resolution, aliased frames*, Proc. of IEEE 1996 National Aerospace and Electronic Conf. NAECON 2 (1996), pp. 702–709.

[13] R. Lagendijk and J. Biemond, *Iterative identification and restoration of images*, Kluwer Academic Publishers, 1991.

[14] J. Lim, *Two-dimensional signal and image processing*, Prentice Hall, 1990.

[15] F. Luk and D. Vandevoorde, *Reducing boundary distortion in image restoration*, Proc. SPIE 2296, Advanced Signal Processing Algorithms, Architectures and Implementations VI, 1994.

[16] S. Kim, N. Bose, and H. Valenzuela, *Recursive reconstruction of high resolution image from noisy undersampled multiframes*, IEEE Trans. on Acoust., Speech, and Signal Process., 38 (1990), pp. 1013–1027.

[17] M. Ng, R. Chan, T. Chan, and A. Yip, *Cosine Transform Preconditioners for High Resolution Image Reconstruction*, Res. Rept. 99-10, Dept. Math., The Chinese University of Hong Kong, or Linear Algebra Appls., to appear.

[18] R. Schultz and R. Stevenson, *Extraction of high-resolution frames from video sequences*, IEEE T. Image Proces., 5 (1996), pp. 996–1011.

[19] G. Strang, *The Discrete Cosine Transform*, SIAM Review, 41 (1999), pp. 135–147.

[20] A. Tekalp, M. Ozkan, and M. Sezan, *High-resolution image reconstruction from lower-resolution image sequences and space-varying image restoration*, In Proc. IEEE Int. Conf. Acoust., Speech, and Signal Process., III, pp. 169–172, San Francisco, CA, March 1992.

[21] R. Tsai and T. Huang, *Multiframe image restoration and registration*, Advances in Computer Vision and Image Processing, 1 (1984), pp. 317–339.

Figure 1: The original image.

Figure 2: (2x2 sensor) A low resolution image (left) and th e observed high resolution image (right)

Figure 3: (2x2 sensor) The reconstructed image using the Ne umann boundary condition.

Figure 4: (2x2 sensor) The reconstructed images using the z ero (left) and the periodic (right) boundary conditions
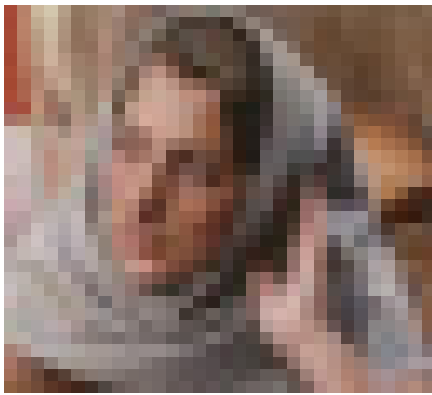

Figure 5: (4x4 sensor) A low resolution image (left) and th e observed high resolution image (right).

Figure 6: (4x4 sensor) The reconstructed image using the Ne umann boundary condition.

21

Figure 7: (4x4 sensor) The reconstructed images using the z ero (left) and the periodic (right) boundary conditions